Complementarity and Internal Consistency between Magnetic and Optical Properties for the $Mn^{II}Cu^{II}$ Heterodinuclear Compound $[Mn(Me_6\text{-}[14]ane\text{-}N_4)Cu(oxpn)](CF_3SO_3)_2$ (Me_6-[14]ane-N_4 = (±)-5,7,7,12,14,14-Hexamethyl-1,4,8,11-tetraazacyclotetradecane; oxpn = *N,N'*-Bis(3-aminopropyl)oxamide)

Corine Mathonière,[1a] Olivier Kahn,*[,1a] Jean-Claude Daran,[1b] Harald Hilbig,[1c] and Frank H. Köhler[1c]

Laboratoire de Chimie Inorganique, URA No. 420, Université de Paris Sud, 91405 Orsay, France, Laboratoire de Chimie des Métaux de Transition, URA No. 419, Université Pierre et Marie Curie, 75232 Paris, France, and Anorganisch-chemisches Institut, Technische Universität München, D-8046 Garching, Germany

Received February 26, 1993

A heterodinuclear compound of formula $[Mn(Me_6\text{-}[14]ane\text{-}N_4)Cu(oxpn)](CF_3SO_3)_2$ (hereafter abbreviated as MnCu), with Me_6-[14]ane-N_4 standing for (±)-5,7,7,12,14,14-hexamethyl-1,4,8,11-tetraazacyclotetradecane and oxpn for *N,N'*-bis(3-aminopropyl)oxamide, has been synthesized. Its crystal structure has been solved. It crystallizes in the monoclinic system, space group $P2_1/a$. The lattice parameters are a = 17.781(7) Å, b = 18.202(5) Å, c = 12.893(4) Å, and β = 105.48(3)° with Z = 4. Its structure consists of oxamido-bridged $Mn^{II}Cu^{II}$ dications and noncoordinated triflate anions. The Mn(II) ion is in distorted octahedral surroundings, and the Cu(II) ion in square-planar surroundings. The intramolecular Mn- - -Cu separation is equal to 5.436 Å. The temperature dependence of the magnetic susceptibility has been investigated in the 300-2 K range and has revealed a ground quintet–excited septet energy gap of $3J$ = –93.9 cm^{-1}. It has also indicated that the zero-field splitting within the quintet state was too small to be detected from the magnetic data. Both NMR and EPR properties have been investigated. The NMR spectrum in CD_3CN solution is poorly resolved. The X-band powder EPR study has allowed the estimation of values of the axial and rhombic zero-field splitting parameters within the S = 2 state. The absorption properties of MnCu have also been investigated. The main feature of the spectrum is a sharp and intense band corresponding to the $^6A_1 \rightarrow {}^4A_1 + {}^4E$ spin-forbidden transition for Mn(II) activated by an exchange mechanism. The temperature dependence of the intensity of this band has offered an alternative method to determine the quintet–septet energy gap.

Introduction

For several years we have been studying $Mn^{II}Cu^{II}$ bimetallic species. Up to now our main efforts have concerned the controlled synthesis of such compounds and the understanding of their magnetic properties.[2] This work has already allowed us to introduce several new concepts in the field of molecular magnetism. Among them we can mention the following: (i) the occurrence of a strong interaction between spin carriers far apart from each other, propagated by conjugated bisbidentate ligands[2] and the spin density delocalization on such ligands;[3] (ii) the irregular spin-state structure;[4] (iii) the one-dimensional ferrimagnetism;[5-7] (iv) the ferromagnetic ordering of high-spin molecules or ferrimagnetic chains.[8-10]

In addition to their magnetic susceptibility and magnetization properties, those systems may present other interesting physical properties. This has proved to be true for EPR.[11-14] We would like to show now that the optical properties are also worth being investigated. A great deal of effort has concerned the spectroscopy of exchange-coupled systems, and quite a few reports deal with heteropairs,[18-31] some of them with $Mn^{II}Cu^{II}$ pairs.[21,22,24] However, up to now, these pairs were obtained in doped systems and not in dinuclear molecular species, so that the information deduced from the optical studies could not be compared to the results of the magnetic studies.

(1) (a) Université de Paris Sud. (b) Université Pierre et Marie Curie. (c) Technische Universität München.
(2) Kahn, O. *Struct. Bonding (Berlin)* **1987**, *68*, 89.
(3) Baron, V.; Gillon, B.; Kahn, O.; Mathonière, C.; Bonnet, M.; Boucherlé, J. X. *Liq. Cryst. Mol. Cryst.* **1993**, in press.
(4) Pei, Y.; Journaux, Y.; Kahn, O. *Inorg. Chem.* **1988**, *27*, 299.
(5) Verdaguer, M.; Julve, M.; Michalowicz, A.; Kahn, O. *Inorg. Chem.* **1983**, *22*, 2624.
(6) Gleizes, A.; Verdaguer, M. *J. Am. Chem. Soc.* **1984**, *106*, 3727.
(7) Pei, Y.; Verdaguer, M.; Kahn, O.; Sletten, J.; Renard, J. P. *Inorg. Chem.* **1987**, *26*, 138.
(8) Kahn, O.; Pei, Y.; Verdaguer, M.; Renard, J. P.; Sletten, J. *J. Am. Chem. Soc.* **1988**, *110*, 782.
(9) Nakatani, K.; Carriat, J. Y.; Journaux, Y.; Kahn, O.; Lloret, F.; Renard, J. P.; Pei, Y.; Sletten, J.; Verdaguer, M. *J. Am. Chem. Soc.* **1988**, *111*, 5739.
(10) Pei, Y.; Kahn, O.; Nakatani, K.; Codjovi, E.; Mathonière, C.; Sletten, J. *J. Am. Chem. Soc.* **1991**, *113*, 6558.
(11) Gatteschi, D.; Guillou, O.; Zanchini, C.; Sessoli, R.; Kahn, O.; Verdaguer, M.; Pei, Y. *Inorg. Chem.* **1989**, *28*, 287.
(12) Gatteschi, D.; Zanchini, C.; Kahn, O.; Pei, Y. *Chem. Phys. Lett.* **1989**, *160*, 157.
(13) Bencini, A.; Gatteschi, D. *EPR of Exchange Coupled Systems*; Springer-Verlag: Berlin, 1989.
(14) Journaux, Y.; Kahn, O.; Morgenstern-Badarau, I.; Galy, J.; Jaud, J.; Bencini, A.; Gatteschi, D. *J. Am. Chem. Soc.* **1985**, *109*, 6305.
(15) Güdel, H. U. in *Magneto-Structural Correlations in Exchange Coupled Systems*; Willett, R. D., Gatteschi, D., Kahn, O., Eds.; Reidel: Dordrecht, The Netherlands, 1985; p 297.
(16) McCarthy, P. J.; Güdel, H. U. *Coord. Chem. Rev.* **1988**, *88*, 69.
(17) Ferguson, J.; Guggenheim, H. J.; Tanabe, Y. *J. Phys. Soc. Jpn.* **1966**, *21*, 692.
(18) Ferguson, J.; Guggenheim, H. J.; Tanabe, Y. *J. Chem. Phys.* **1966**, *45*, 1134.
(19) Ferguson, J.; Guggenheim, H. J.; Tanabe, Y. *Phys. Rev.* **1967**, *161*, 207.
(20) Ferguson, J.; Güdel, H. U.; Krausz, E. R. *Mol. Phys.* **1975**, *30*, 1139.
(21) Ferguson, J.; Guggenheim, H. J. *Phys. Rev. B* **1970**, *1*, 4223.
(22) Ferguson, J.; Guggenheim, H. J.; Krausz, E. R. *J. Phys. C: Solid State Phys.* **1971**, *4*, 1866.
(23) Ferguson, J.; Fielding, P. E. *Aust. J. Chem.* **1972**, *25*, 1371.
(24) Ferré, J.; Regis, M. *Solid State Commun.* **1978**, *26*, 225.
(25) Ferguson, J.; Masui, H. *J. Lumin.* **1979**, *18–19*, 224.
(26) Wiltshire, M. C. K. *J. Phys. C: Solid State Phys.* **1982**, *15*, 4177.
(27) Wood, T. E.; Cox, P. A.; Day, P.; Walker, X. *J. Phys. C: Solid State Phys.* **1982**, *15*, L787.
(28) Jacobsen, S. M.; Güdel, H. U.; Smith, W. E. *Inorg. Chem.* **1987**, *26*, 2001.
(29) Herren, M.; Jacobsen, S. M.; Güdel, H. U.; Briat, B. *J. Chem. Phys.* **1989**, *2*, 663.
(30) Herren, M.; Jacobsen, S. M.; Güdel, H. U. *Inorg. Chem.* **1989**, *28*, 504.
(31) Herren, M.; Güdel, H. U. *J. Lumin.* **1993**, in press.

0020-1669/93/1332-4057$04.00/0

This paper deals with the simplest case of $Mn^{II}Cu^{II}$ dinuclear compound, that of a dinuclear unit. When we decided to undertake this work we realized that we had very few genuine $Mn^{II}Cu^{II}$ pairs at our disposal and that none of them were suitable for the kind of study we had in mind. For instance, we recently described the compound $MnCu(Cl_5obbz)(H_2O)_5$ with Cl_5obbz = oxamido-*N*,*N*′-bis(3,5-dichlorobenzoato). Its structure consists of carboxylato-bridged dinuclear units. However, the interaction between the Mn(II) and Cu(II) ions is negligibly small;[32] to a large extent the physics of this dinuclear entity is just the superposition of what arises from the Mn(II) and Cu(II) chromophores. Moreover the presence of aromatic rings within the ligand provokes an intense $\pi \rightarrow \pi^*$ transition at the frontier between UV and visible ranges. This transition hides narrow bands which proved to provide very important information for the $Mn^{II}Cu^{II}$ systems. As a consequence of this, we synthesized a new dinuclear species, with a strong intramolecular interaction between the metal centers. For that, we used ligands which do not present any band on their own in the frequency range of interest, namely 300–900 nm. In this paper we will first describe the synthesis and the crystal structure of this compound hereafter abbreviated as MnCu. Its formula is $[Mn(Me_6\text{-}[14]ane\text{-}N_4)Cu(oxpn)](CF_3SO_3)_2$, Me_6-[14]ane-N_4 standing for (±)-5,7,7,12,14,14-hexamethyl-1,4,8,11-tetraazacyclotetradecane and oxpn for *N*,*N*′-bis(3-aminopropyl)oxamide. Then we will successively investigate the magnetic susceptibility, NMR, EPR, and optical properties of this compound. We will see that in the meantime there are an internal consistency and a complementarity between these various techniques.

Experimental Section

Synthesis. The organic molecules Me_6-[14]ane-N_4 and H_4oxpn were synthesized as previously described.[33,34] The synthesis of $[Mn(Me_6\text{-}[14]ane\text{-}N_4)](CF_3SO_3)_2$ has also been reported.[35] The copper(II) precursor Cu(oxpn) was prepared according to a method slightly modified with respect to that already described.[36] A 4-mmol amount of NaOH dissolved in 10 mL of water was added to 2 mmol of H_4oxpn dissolved in 10 mL of water. The mixture was stirred, and then 2 mmol of copper(II) nitrate dissolved in 10 mL of water was added. After 0.5 h the water was evaporated almost to dryness, and 50 mL of ethanol was poured on the residue. Cu(oxpn) was obtained as a red precipitate, filtered off, and washed with ethanol. The synthesis of $[Mn(Me_6\text{-}[14]ane\text{-}N_4)Cu(oxpn)](CF_3SO_3)_2$ was carried out under argon in Schlenk tubes. A 0.2-mmol amount (122 mg) of $[Mn(Me_6\text{-}[14]ane\text{-}N_4)](CF_3SO_3)_2$ dissolved in 20 mL of acetonitrile was added to 0.2 mmol (53 mg) of Cu(oxpn) dispersed in methanol. The mixture was stirred until the solution became limpid. This solution was then filtered and reduced by evaporation to a few milliliters. Red well-shaped single crystals were obtained within a few days by aerial diffusion of diethyl oxide into the solution. Anal. Calcd for $C_{26}H_{52}N_8O_8F_6S_2CuMn$: C, 34.65; H, 5.60; N, 12.43; F, 12.65; Cu, 7.05; Mn, 6.10. Found: C, 34.70; H, 5.82; N, 12.41; F, 12.62; Cu, 6.90; Mn, 6.01.

X-ray Data Collection and Structure Determination. A selected crystal was set up on an automatic diffractometer. Unit cell dimensions were obtained from least-squares refinements of the setting angles of 25 well-centered reflections. Two standard reflections were monitored periodically and showed no change of intensity during data collection. Crystallographic data and other pertinent information are summarized in Table I. Corrections were made for Lorentz and polarization effects. Empirical absorption corrections (Difabs[37]) were applied. Computations were performed by using CRYSTALS[38] adapted on a MicroVax II. Atomic factors for neutral Cu, Mn, S, O, N, C, and H atoms were taken from ref 39. Anomalous dispersion was taken into account. The structure was solved by direct methods using the SHELX86 program.[39] One of the two triflate anions appeared to be disordered. As a matter of fact, the thermal parameters for the fluorine and oxygen atoms acquired large values, and the difference electron density map revealed several peaks in the immediate vicinity of this anion. Several attempts to model this disorder were unsuccessful, so that the original model of just one position for this triflate anion was adopted. However, the distances and angles within this CF_3SO_3 group were restrained to chemically reasonable values (C–F = 1.30 Å, S–O = 1.40 Å, C–S = 1.80 Å, O–S–C = 109°, F–S–C = 109°). The hydrogen atoms were found on difference electron density maps but were introduced in the refinement as fixed contributors in calculated positions. Their position coordinates were recalculated after each cycle. They were given isotropic thermal parameters 20% higher than those of the carbon atoms to which they are bound. Anisotropic temperature factors were introduced for all non-hydrogen atoms. Least-squares refinements with approximation to the normal matrix were carried out by minimizing the function $\sum w(|F_o| - (|F_c|)^2$, where F_o and F_c are the observed and calculated structure factors, respectively. The weighting scheme used in the last refinement cycle was $w = w'[1 - (\Delta F/6\sigma(F_o))^2]^2$ where $w' = 1/\sum^3 \mathrm{ArTr}(x)$ with three coefficients Ar for the Chebyshev polynomial $\mathrm{ArTr}(x)$, x being $F_o/F_c(\max)$.[40] The convergence was reached with R and R_w values listed in Table I. Criteria for a satisfactory complete analysis were the ratios of root-mean-square shift to standard deviation being less than 0.1 and no significant features in the final difference maps. Atomic coordinates are given in Table II, interatomic distances in Table III, and bond angles in Table IV.

Table I. Crystallographic Data

chem formula	$C_{26}H_{52}F_6N_8S_2CuMn$	fw	901.3
a, Å	17.781(7)	space group	$P2_1/a$
b, Å	18.202(5)	λ, Å	0.710 70 (MoKα)
c, Å	12.893(4)	ρ(calcd), g·cm^{-3}	1.49
β, deg	105.48(3)	μ(Mo Kα), cm^{-1}	10.08
V, Å^3	4022(32)	$R(F_o)$	0.052
Z	4	$R_w(F_o)$	0.065
T, °C	23		

Magnetic Measurements. These were carried out with two apparatuses, a Faraday-type magnetometer equipped with a helium continuous-flow cryostat working down to 4.2 K and a low-field SQUID magnetometer working in the 2–20 K temperature range. Diamagnetic correction was estimated as -440×10^{-6} cm^3 mol^{-1}.

Magnetic Resonance. The NMR spectra in CD_3CN were obtained with a Bruker MSL 300 spectrometer. The EPR spectra were recorded on powder samples at various temperatures down to 4.2 K with a Bruker 200 D EPR spectrometer equipped of a continuous-flow cryostat, a Hall probe, and a frequency meter.

Optical Spectra. These were recorded with a Varian 2300 spectrometer equipped with a closed-circuit cryostat provided by Air Products. The spectra were studied both in acetonitrile solution and as KBr pellets fixed on a copper plate with silver paint. The lowest temperature which can be reached is 10 K. The band intensities were calculated from the area delimited by the absorption bands and a baseline common to all spectra.

Description of the Structure

The structure consists of isolated $[Mn(Me_6\text{-}[14]ane\text{-}N_4)Cu(oxpn)]^{2+}$ cations and triflate anions. A perspective view of the heterodinuclear cation along with the atom-labeling scheme is shown in Figure 1. The manganese atom is in a distorted octahedral environment, being linked to the four nitrogen atoms of the Me_6-[14]ane-N_4 ligand (average Mn–N bond length = 2.266 Å) and the two oxygen atoms of the oxamido group (average Mn–O bond length = 2.172 Å). The copper atom is in a slightly distorted square-planar environment; it is linked to the four nitrogen atoms of the oxpn group. The Cu–N(1) and Cu–N(2) bond lengths involving the amide nitrogen atoms (1.953(4) and 1.941(4) Å) are significantly shorter than the Cu–N(3) and Cu–N(4) bond lengths involving the amine nitrogen atoms (2.016(4) and 2.017(4) Å).

(32) Nakatani, K.; Sletten, J.; Halut-Desporte, S.; Jeannin, S.; Jeannin, Y.; Kahn, O. *Inorg. Chem.* **1991**, *30*, 164.
(33) Tait, A. M.; Bush, D. H. *Inorg. Nucl. Chem. Lett.* **1972**, *8*, 491.
(34) Chang, H. J.; Volg, A. *J. Polym. Sci.* **1977**, *15*, 311.
(35) Bryan, P. S.; Dabrowiak, J. C. *Inorg. Chem.* **1975**, *14*, 296.
(36) Journaux, Y.; Sletten, J.; Kahn, O. *Inorg. Chem.* **1986**, *25*, 439.
(37) Walker, N.; Stuart, D. *Acta Crystallogr.* **1983**, *39*, 158.
(38) Watkin, D. J.; Carruthers, J. R.; Betteridge, P. W. *CRYSTALS, A, Advanced Crystallographic Program System*; Oxford, U.K., 1988.
(39) *International Tables for X-Ray Crystallography*; Kynoch Press: Birmingham, U.K., 1974; Vol. IV.
(40) Prince, E. *Mathematical Techniques in Crystallography*; Springer-Verlag: Berlin, 1982.

Table II. Fractional Atomic Coordinates with Esd's in Parentheses and Equivalent Isotropic Thermal Parameter U(eq)

atom	x/a	y/b	z/c	U(eq),[a] Å^2
Cu(1)	0.37010(3)	0.17024(3)	0.07997(4)	0.0461
Mn(1)	0.39306(4)	0.26283(4)	−0.31118(5)	0.0427
O(1)	0.3072(2)	0.2331(2)	−0.2259(2)	0.0496
O(2)	0.4642(2)	0.2345(2)	−0.1519(3)	0.0525
O(11)	0.8324(4)	0.6100(3)	0.2769(6)	0.1080
O(12)	0.8214(3)	0.4813(3)	0.2521(4)	0.0852
O(13)	0.9343(3)	0.5440(4)	0.2322(5)	0.1104
O(21)	0.4711(6)	0.3197(6)	0.269(1)	0.2346
O(22)	0.3671(4)	0.2727(3)	0.3246(4)	0.1038
O(23)	0.4257(5)	0.3833(3)	0.3929(4)	0.1283
N(1)	0.2998(2)	0.1931(2)	−0.0607(3)	0.0478
N(2)	0.4515(2)	0.1899(3)	0.0090(3)	0.0551
N(3)	0.4452(3)	0.1384(3)	0.2193(4)	0.0647
N(4)	0.2830(3)	0.1625(3)	0.1526(3)	0.0559
N(5)	0.4883(2)	0.3074(2)	−0.3793(3)	0.0489
N(6)	0.4334(2)	0.1566(2)	−0.3721(3)	0.0485
N(7)	0.3529(2)	0.3811(2)	−0.3088(3)	0.0504
N(8)	0.2995(2)	0.2654(2)	−0.4692(3)	0.0457
C(1)	0.3366(2)	0.2138(2)	−0.1299(3)	0.0423
C(2)	0.4254(2)	0.2134(3)	−0.0886(4)	0.0464
C(3)	0.5355(3)	0.1859(6)	0.0536(6)	0.0838
C(4)	0.5592(5)	0.146(1)	0.1513(9)	0.1170
C(5)	0.5298(4)	0.1391(6)	0.2323(7)	0.0929
C(6)	0.2153(3)	0.1913(4)	−0.0953(4)	0.0623
C(7)	0.1804(4)	0.1617(7)	−0.0134(6)	0.0914
C(8)	0.2033(4)	0.1787(6)	0.0928(6)	0.0867
C(9)	0.5378(3)	0.2429(3)	−0.3810(5)	0.0575
C(10)	0.4881(3)	0.1800(3)	−0.4356(4)	0.0569
C(11)	0.3732(3)	0.1016(3)	−0.4262(4)	0.0530
C(12)	0.3106(3)	0.1355(3)	−0.5180(4)	0.0556
C(13)	0.2562(3)	0.1955(3)	−0.4962(4)	0.0531
C(14)	0.2494(3)	0.3279(3)	−0.4549(5)	0.0575
C(15)	0.2997(3)	0.3950(3)	−0.4150(5)	0.0575
C(16)	0.4142(3)	0.4392(3)	−0.2684(5)	0.0565
C(17)	0.4762(3)	0.4379(3)	−0.3324(5)	0.0607
C(18)	0.5316(3)	0.3732(3)	−0.3225(4)	0.0565
C(20)	0.8079(5)	0.5595(5)	0.0866(7)	0.0971
C(21)	0.3426(4)	0.3826(3)	0.1979(5)	0.1577
C(111)	0.4104(4)	0.0371(3)	−0.4724(5)	0.0652
C(112)	0.3385(4)	0.0716(3)	−0.3386(5)	0.0676
C(131)	0.1849(3)	0.2041(4)	−0.5944(5)	0.0718
C(161)	0.4508(4)	0.4234(4)	−0.1499(5)	0.0753
C(162)	0.3783(4)	0.5154(3)	−0.2810(7)	0.0763
C(181)	0.5996(4)	0.3949(4)	−0.3689(6)	0.0797
S(1)	0.85401(9)	0.54792(8)	0.2279(1)	0.0658
S(2)	0.4053(1)	0.3351(1)	0.3061(1)	0.0832
F(11)	0.7311(3)	0.5593(5)	0.0697(5)	0.1417
F(12)	0.8264(4)	0.6199(3)	0.0473(6)	0.1339
F(13)	0.8257(4)	0.5046(4)	0.0307(4)	0.1380
F(21)	0.3702(6)	0.4438(3)	0.1769(5)	0.1408
F(22)	0.3305(6)	0.3392(3)	0.1146(5)	0.1635
F(23)	0.2777(5)	0.3938(7)	0.222(1)	0.2983

[a] $U(\text{eq}) = [U_{11}U_{22}U_{33}]^{1/3}$.

The two metal ions are linked by an oxamido bridge, O(1)O(2)C(1)C(2)N(1)N(2), the Mn- - -Cu separation being equal to 5.436 Å. Within the bridge the C–O and C–N bonds have some double-bond character. On the other hand, the central C(1)–C(2) bond length, 1.527(6) Å, is characteristic of a single bond. The Mn, Cu, O(1), O(2), C(1), C(2), N(1), and N(2) atoms are almost coplanar, the deviations with respect to the mean plane being in the range 0.02–0.058 Å. It turns out that the molecular symmetry is very close to C_{2v}.

The dinuclear cations are well separated from each other within the lattice by the triflate ions. All Cu- - -O(triflate) separations are larger than 3 Å, which is in line with the fact that the copper atom is located within its basal plane and not pulled out of this plane toward an apical site.

Magnetic Properties

The magnetic behavior of $[Mn(Me_6\text{-}[14]ane\text{-}N_4)Cu(oxpn)](CF_3SO_3)_2$ is represented in Figure 2 in the form of the $\chi_M T$ versus T plot, χ_M being the molar magnetic susceptibility and T the temperature. This behavior is quite characteristic of an antiferromagnetically coupled $Mn^{II}Cu^{II}$ pair. At room temperature $\chi_M T$ is equal to 4.32 cm^3 K mol^{-1}, a value which is

Table III. Bond Distances (Å)[a]

Cu(1)–N(1)	1.953(4)	Cu(1)–N(3)	2.016(4)
Cu(1)–N(2)	1.941(4)	Cu(1)–N(4)	2.017(4)
Mn(1)–O(1)	2.175(3)	Mn(1)–N(6)	2.275(4)
Mn(1)–O(2)	2.168(3)	Mn(1)–N(7)	2.272(4)
Mn(1)–N(5)	2.257(4)	Mn(1)–N(8)	2.261(4)
O(1)–C(1)	1.259(5)	O(2)–C(2)	1.260(6)
N(1)–C(1)	1.295(6)	N(2)–C(2)	1.293(6)
C(1)–C(2)	1.527(6)		
N(1)–C(6)	1.449(6)	N(3)–C(5)	1.469(8)
N(2)–C(3)	1.451(7)	N(4)–C(8)	1.451(8)
C(3)–C(4)	1.42(1)	C(6)–C(7)	1.462(9)
C(4)–C(5)	1.29(1)	C(7)–C(8)	1.36(1)
N(5)–C(9)	1.471(6)	N(7)–C(15)	1.464(7)
N(5)–C(18)	1.504(7)	N(7)–C(16)	1.508(7)
N(6)–C(10)	1.491(7)	N(8)–C(13)	1.480(6)
N(6)–C(11)	1.496(6)	N(8)–C(14)	1.486(6)
C(9)–C(10)	1.503(8)	C(14)–C(15)	1.521(8)
C(11)–C(12)	1.522(7)	C(16)–C(17)	1.543(8)
C(11)–C(111)	1.543(7)	C(16)–C(161)	1.520(9)
C(11)–C(112)	1.525(8)	C(16)–C(162)	1.518(8)
C(12)–C(13)	1.535(7)	C(17)–C(18)	1.518(8)
C(13)–C(131)	1.543(7)	C(18)–C(181)	1.537(8)

[a] Esd's in parentheses refer to the last significant digit.

Table IV. Bond Angles (deg)[a]

N(2)–Cu(1)–N(1)	84.0(2)	N(4)–Cu(1)–N(1)	93.7(2)
N(3)–Cu(1)–N(1)	174.9(2)	N(4)–Cu(1)–N(2)	173.3(2)
N(3)–Cu(1)–N(2)	94.2(2)	N(4)–Cu(1)–N(3)	88.5(2)
O(2)–Mn(1)–O(1)	76.9(1)		
N(5)–Mn(1)–O(1)	170.9(1)	N(7)–Mn(1)–N(5)	86.3(1)
N(5)–Mn(1)–O(2)	98.4(1)	N(7)–Mn(1)–N(6)	160.1(2)
N(6)–Mn(1)–O(1)	106.9(1)	N(8)–Mn(1)–O(1)	90.8(1)
N(6)–Mn(1)–O(2)	88.1(1)	N(8)–Mn(1)–O(2)	164.1(1)
N(6)–Mn(1)–N(5)	80.4(1)	N(8)–Mn(1)–N(5)	95.2(1)
N(7)–Mn(1)–O(1)	87.9(1)	N(8)–Mn(1)–N(6)	86.0(1)
N(7)–Mn(1)–O(2)	108.6(2)	N(8)–Mn(1)–N(7)	80.5(1)
C(1)–O(1)–Mn(1)	113.8(3)	C(2)–O(2)–Mn(1)	113.9(3)
C(1)–N(1)–Cu(1)	112.7(3)	C(2)–N(2)–Cu(1)	113.6(3)
C(6)–N(1)–Cu(1)	129.4(3)	C(3)–N(2)–Cu(1)	128.5(4)
C(6)–N(1)–C(1)	117.8(4)	C(3)–N(2)–C(2)	117.8(4)
C(5)–N(3)–Cu(1)	120.9(4)	C(8)–N(4)–Cu(1)	120.0(4)
C(9)–N(5)–Mn(1)	103.4(3)	C(10)–N(6)–Mn(1)	105.0(3)
C(18)–N(5)–Mn(1)	115.9(3)	C(11)–N(6)–Mn(1)	118.6(3)
C(18)–N(5)–C(9)	114.4(4)	C(11)–N(6)–C(10)	115.2(4)
C(15)–N(7)–Mn(1)	106.1(3)	C(13)–N(8)–Mn(1)	113.9(3)
C(16)–N(7)–Mn(1)	117.9(3)	C(14)–N(8)–Mn(1)	103.0(3)
C(16)–N(7)–C(15)	115.4(4)	C(14)–N(8)–C(13)	113.3(4)
N(1)–C(1)–O(1)	127.3(4)	N(2)–C(2)–O(2)	128.0(4)
C(2)–C(1)–O(1)	117.6(4)	C(1)–C(2)–O(2)	117.8(4)
C(2)–C(1)–N(1)	115.1(4)	C(1)–C(2)–N(2)	114.2(4)
C(4)–C(3)–N(2)	114.1(6)	C(7)–C(6)–N(1)	113.0(5)
C(5)–C(4)–C(3)	132.6(10)	C(8)–C(7)–C(6)	125.0(8)
C(4)–C(5)–N(3)	122.1(7)	C(7)–C(8)–N(4)	118.5(7)
C(10)–C(9)–N(5)	109.6(4)	C(15)–C(14)–N(8)	109.8(4)
C(9)–C(10)–N(6)	110.4(4)	C(14)–C(15)–N(7)	110.6(4)
C(12)–C(11)–N(6)	112.1(4)	C(17)–C(16)–N(7)	111.1(4)
C(111)–C(11)–N(6)	111.2(4)	C(161)–C(16)–N(7)	106.9(5)
C(111)–C(11)–C(12)	108.0(4)	C(161)–C(16)–C(17)	111.1(5)
C(112)–C(11)–N(6)	105.9(4)	C(162)–C(16)–N(7)	111.0(4)
C(112)–C(11)–C(12)	111.4(5)	C(162)–C(16)–C(17)	107.3(5)
C(112)–C(11)–C(111)	108.3(5)	C(162)–C(16)–C(161)	109.6(5)
C(13)–C(12)–C(11)	120.8(4)	C(18)–C(17)–C(16)	120.4(5)
C(12)–C(13)–N(8)	109.9(4)	C(17)–C(18)–N(5)	110.0(4)
C(131)–C(13)–N(8)	111.6(4)	C(181)–C(18)–N(5)	111.6(5)
C(131)–C(13)–C(12)	110.0(4)	C(181)–C(18)–C(17)	109.2(5)

[a] Esd's in parentheses refer to the last significant digit.

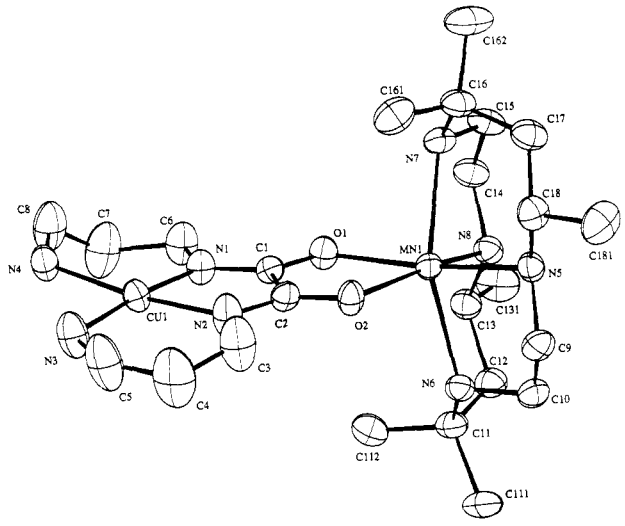

Figure 1. Perspective view of the dinuclear cation in $[Mn(Me_6\text{-}[14]ane\text{-}N_4)Cu(oxpn)](CF_3SO_3)_2$.

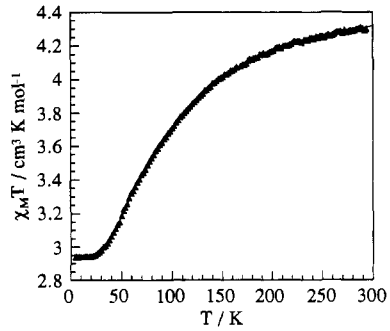

Figure 2. $\chi_M T$ versus T plot for $[Mn(Me_6\text{-}[14]aneN_4)Cu(oxpn)](CF_3SO_3)_2$: (▲) experimental points; (—) calculated curve.

slightly below what would be anticipated for isolated Mn(II) and Cu(II) ions with $S_{Mn} = {}^5/_2$ and $S_{Cu} = {}^1/_2$ local spins. As T is lowered, $\chi_M T$ decreases down to ca. 25 K and then reaches a plateau below this temperature with $\chi_M T = 2.94$ cm³ K mol⁻¹. This plateau corresponds to the temperature range where only the quintet ground state is thermally populated. The presence of this plateau in the low-temperature range indicates that the zero-field splitting within the $S = 2$ ground state is too small to be detected by magnetic data down to 2 K. This situation will have important consequences as far as the EPR properties are concerned (vide infra).

The magnetic properties of $[Mn(Me_6\text{-}[14]ane\text{-}N_4)Cu(oxpn)](CF_3SO_3)_2$ may be quantitatively interpreted with the theoretical expression for the magnetic susceptibility of a Mn^{II}-Cu^{II} pair. This expression is

$$\chi_M T = (2N\beta^2/k)[5g_2^2 + 14g_3^2 \exp(3J/kT)]/[5 + 7\exp(3J/kT)] \quad (1)$$

J is the interaction parameter occurring in the interaction Hamiltonian $-J\mathbf{S}_{Mn}\cdot\mathbf{S}_{Cu}$. The interaction between the Mn(II) and Cu(II) ions gives rise to $S = 2$ and $S = 3$ pair states, with a quintet–septet energy gap of $3J$. g_2 and g_3 in eq 1 are the Zeeman factors associated with the $S = 2$ and $S = 3$ pair states, respectively; they are related to the local Zeeman factors g_{Mn} and g_{Cu} through[13,41]

$$g_2 = (7g_{Mn} - g_{Cu})/6 \qquad g_3 = (5g_{Mn} + g_{Cu})/6 \quad (2)$$

The least-squares fitting of the experimental data leads to $J = -31.3$ cm⁻¹, $g_2 = 1.978$, and $g_3 = 2.022$. The local factors g_{Mn} and g_{Cu} are then found as 2.00 and 2.13, respectively. The agreement factor defined as $\sum[(\chi_M T)^{cal} - (\chi_M T)^{obs}]^2/\sum[(\chi_M T)^{obs}]^2$ is then equal to 6×10^{-6} (for 158 experimental points), which corresponds to an almost perfect agreement. The quintet–septet energy gap is then equal to $3J = -93.9$ cm⁻¹.

(41) Scaringe, R. P.; Hodgson, D.; Hatfield, W. E. *Mol. Phys.* **1978**, *35*, 701.

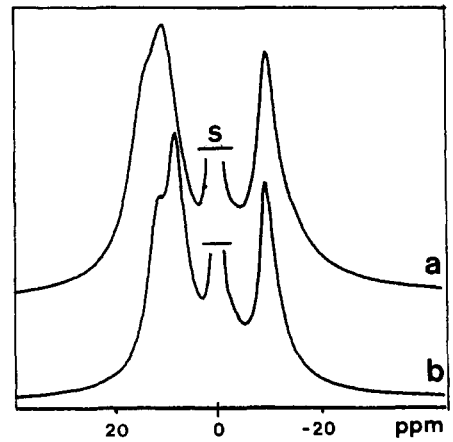

Figure 3. 300-MHz ^{1}H NMR spectra in CD_3CN solution of $[Mn(Me_6\text{-}[14]ane\text{-}N_4)Cu(oxpn)](CF_3SO_3)_2$ at (a) 304 K and (b) 352 K. S = solvent.

NMR and EPR Properties

Generally, the Mn(II) ions in octahedral surroundings and the Cu(II) ions in square-planar surroundings are known to have long electron spin relaxation times. These, in turn, lead to nuclear spin relaxation times which are very unfavorable for NMR spectroscopy.[42] However, when the symmetry at Mn(II) is lowered by replacing, e.g., water with more complicated and stronger binding ligands, the electron relaxation rate may be increased considerably.[43] For instance, one of us and others have undertaken detailed multinuclear NMR studies of various bis(cyclopentadienyl)manganese derivatives.[44] In the present case the distortion of the environment of Mn(II) revealed by X-ray analysis also suggested an increased electron relaxation rate which was expected to be transmitted to Cu(II) by the appreciable antiferromagnetic coupling.[45,46] The ^{1}H NMR spectra of MnCu at 304 and 352 K are shown in Figure 3; no other signal could be detected between 2300 and −1800 ppm. Only two signals at −7.7 and 11.9 ppm together with a shoulder at ca. 15 ppm (all relative to the signal of CHD_2CN) are visible at 304 K. At 352 K the resolution is somewhat better and the signals have moved to −7.3, 9.8, and 12.8 ppm. The temperature dependence confirms that these signals are paramagnetic in origin. The fact that they are weak points to a rather limited electron spin delocalization. Together with the large signal widths this leads to strong overlap and hence fewer nonassignable signals than expected. No details of the spin delocalization may be derived, except that both negative and positive spin density reaches the protons.[47] It turns out that the distorsion at Mn(II) and the related acceleration of the electron relaxation is not sufficient to obtain well-resolved NMR spectra.

The X-band powder EPR spectrum of MnCu is shown in Figure 4. This spectrum was recorded at 10 K, a temperature where only the quintet ground state is thermally populated. The fact that MnCu is not EPR silent confirms that the zero-field splitting within the $S = 2$ state is much weaker than the incident quantum.

(42) Bloembergen, N.; Morgan, L. O. *J. Chem. Phys.* **1961**, *34*, 842.
(43) Cohn, M.; Townsend, J. *Nature (London)* **1954**, *173*, 1091.
(44) Köhler, F. H.; Schlesinger, B. *Inorg. Chem.* **1992**, *31*, 2853 and references therein.
(45) Dei, A.; Gatteschi, D.; Piergentili, E. *Inorg. Chem.* **1979**, *18*, 89.
(46) Bertini, I.; Lanini, G.; Luchinat, C.; Manchini, M.; Spina, G. *J. Magn. Reson.* **1985**, *63*, 56.
(47) We have not attempted to analyze the data quantitatively by, e.g., including dipolar shifts.

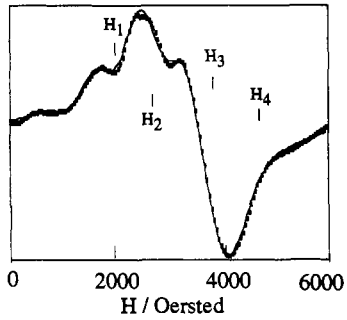

Figure 4. X-Band powder EPR spectrum of [Mn(Me$_6$-[14]ane-N$_4$)-Cu(oxpn)](CF$_3$SO$_3$)$_2$: (···) experimental spectrum at 10 K; (—) simulated spectrum.

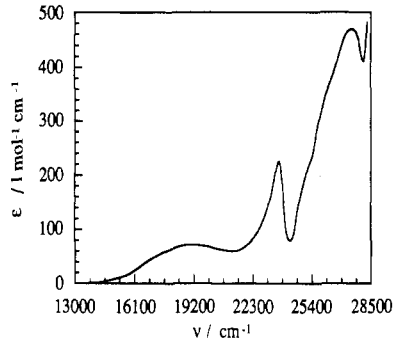

Figure 5. Absorption spectrum in acetonitrile solution of [Mn(Me$_6$-[14]ane-N$_4$)Cu(oxpn)](CF$_3$SO$_3$)$_2$.

The spectrum shows the characteristic features of a $S = 2$ state[48,49] with four allowed transitions around 2000, 2690, 3540, and 4700 Oe and a weak feature around 600 Oe.

The spin Hamiltonian associated with the $S = 2$ pair ground state may be written as

$$\mathcal{H} = \beta H \cdot \mathbf{g}_2 \cdot \mathbf{S} + \mathbf{S} \cdot \mathbf{D}_2 \cdot \mathbf{S} \qquad (3)$$

where $\mathbf{g}_2$ and $\mathbf{D}_2$ are the Zeeman and zero-field splitting tensors within the $S = 2$ state, respectively, and S is the spin operator. It is not possible to deduce the principal values and directions of $\mathbf{g}_2$ and $\mathbf{D}_2$ from a powder spectrum. On the other hand, assuming that $\mathbf{g}_2$ is isotropic with the principal value g_2 (=1.978) deduced from the magnetic susceptibility curve, the axial D ($=3D_{2,zz}/2$) zero-field splitting parameters may be estimated owing to successive comparisons between experimental and simulated powder spectra. $|D|$ was found to be 0.042(6) cm^{-1}. Experimental and simulated powder spectra are compared in Figure 4.

It is worth recalling that $\mathbf{D}_2$ is related to the Mn(II) local anisotropy tensor, $\mathbf{D}_{Mn}$, and the anisotropic interaction tensor, $\mathbf{D}_{MnCu}$, through

$$\mathbf{D}_2 = 4\mathbf{D}_{Mn}/3 - \mathbf{D}_{MnCu}/6 \qquad (4)$$

Due to the large Mn- - -Cu separation, $\mathbf{D}_{Mn}$ is probably the dominant term in the right-hand size of eq 3, which suggests that the axial zero-field splitting parameter for Mn(II) in its distorted octahedral environment is of the order of $D_{Mn} = 3 \times 10^{-2}$ cm^{-1}.

The origin of the feature around 600 Oe is still unclear. Our simulations suggest that it could be due to a $S = 2 \rightarrow S = -1$ transition.

Optical Properties

The absorption spectrum of MnCu at room temperature in acetonitrile solution is shown in Figure 5. This spectrum displays a broad band at 520 nm (19 231 cm^{-1}; ϵ = 71 L mol^{-1} cm^{-1}), a rather intense and narrow band at 422 nm (23 697 cm^{-1}; ϵ = 225 L mol^{-1} cm^{-1}), and two other narrow features at 382 nm (26 178 cm^{-1}) and 361 nm (27 701 cm^{-1}). The band at 520 nm is characteristic of copper(II) in square-planar environment.[50] It corresponds to the $^2B_1 \rightarrow {}^2A_1$ local transition in C_{2v} site symmetry. The narrow bands in the high-energy range of the spectrum correspond to formally spin-forbidden transitions of manganese(II). Their relatively strong intensities indicate that they are activated by an exchange mechanism. We will come back on this essential point later on. The beautifully shaped band at 422 nm can be unambiguously assigned to the $^6A_1 \rightarrow {}^4A_1 + {}^4E$ transition of manganese(II). In octahedral surroundings the $^4A_1$ and ^4E states arising from ^4G remain degenerate, and the energy of this transition is not influenced at the first order by the ligand field, as there is no electron jump between the t_{2g} and e_g orbitals. By analogy with the spectra of other octahedral Mn(II) species, the other two bands can be assigned to $^6A_1 \rightarrow {}^4T_2(D)$ and $^6A_1 \rightarrow {}^4E(D)$ transitions.[50] It is worth mentioning that the metal- - - metal charge-transfer bands, if they did exist, could not be detected. Indeed, they would be hidden by the high-energy ligand- - -metal charge-transfer bands.

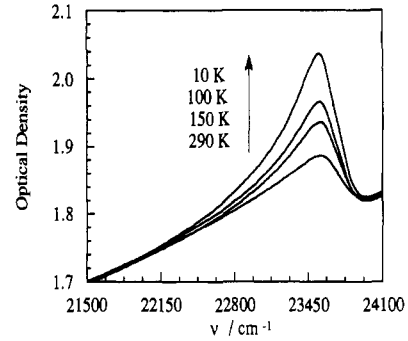

Figure 6. Absorption band at 422 nm for [Mn(Me$_6$-[14]ane-N$_4$)Cu(oxpn)](CF$_3$SO$_3$)$_2$ in KBr pellets.

The temperature dependence of the intensity of the narrow band at 422 nm offers an alternative means to determine the J exchange parameter. The coupling between the Mn(II) and Cu(II) ground local states gives rise to two low-lying pair states characterized by the spins $S = 2$ and $S = 3$. If we assume a somewhat idealized C_{2v} symmetry for the metal sites and the dinuclear entity as a whole, then the ground local states may be labeled as $^6A_1$ and $^2B_1$ and the low-lying pair states as $^5B_1$ and $^7B_1$. The coupling between the spin-quartet excited state for Mn(II) and the ground state for Cu(II) gives rise to two excited pair states characterized by the spins $S^* = 1$ and $S^* = 2$. Due to the degeneracy of the $^4A_1 + {}^4E$ excited states for Mn(II) in octahedral surroundings, the symmetry labels of the two excited pair states in C_{2v} symmetry are $^3A_1 + 2^3B_1$ for $S^* = 1$, and $^5A_1 + 2^5B_1$ for $S^* = 2$. Only the $S = 2 \rightarrow S^* = 2$ transition between pair states is spin-allowed as schematized in the insert of Figure 7. Therefore, the intensity I of the observed transition varies as the thermal population of the ground $S = 2$ state, i.e. as

$$I = 5I_0/[(5 + 7\exp(3J/kT)] \qquad (5)$$

where I_0 is the intrinsic intensity of the $S = 2 \rightarrow S^* = 2$ transition. The band at 422 nm was recorded at various temperatures between 10 and 300 K on a KBr pellet containing 3% MnCu. Typical spectra at four temperatures are displayed in Figure 6. As expected the intensity decreases as the temperature increases. Figure 7 shows the temperature dependence of the intensity I together with the best theoretical curve obtained by minimizing the agreement factor defined as $\sum[(I/I_0)^{obs} - (I/I_0)^{cal}]^2/\sum[(I/I_0)^{obs}]^2$, where I_0 is taken as the intensity at 10 K. J is then found as −30.5 cm^{-1}. This value within the experimental uncertainties is identical to that deduced from the magnetic data.

(48) Pauson, J. A.; Krost, D. A.; McPherson, G. L.; Rogers, R. D.; Atwood, J. L. *Inorg. Chem.* **1980**, *19*, 2519.
(49) Banci, L.; Bencini, A.; Gatteschi, D. *Inorg. Chem.* **1981**, *20*, 2734.
(50) Lever, A. B. P. *Inorganic Electronic Spectroscopy*, 2nd ed.; Elsevier: Amsterdam, 1984.

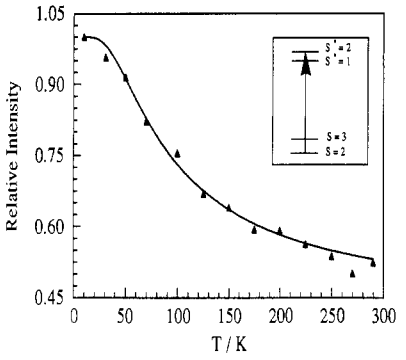

Figure 7. Temperature dependence of the absorption band at 422 nm for $[Mn(Me_6\text{-}[14]ane\text{-}N_4)Cu(oxpn)](CF_3SO_3)_2$: (▲) experimental data; (—) calculated curve.

Conclusion

To the best of our knowledge, this is the first paper in which information concerning the magnitude of the interaction in an heterodinuclear system is deduced from both magnetic and optical properties. The previously unknown $[Mn(Me_6\text{-}[14]ane\text{-}N_4)Cu(oxpn)](CF_3SO_3)_2$ has been tailor-made to test the internal consistency between magnetic and optical data. Some related compounds had been reported by a Chinese group.[51] The interaction between Mn(II) and Cu(II) ions in a dinuclear compound gives rise to two low-lying states, so that the temperature dependence of the magnetic susceptibility only depends on the energy gap between these two states and not on any phenomenological spin-coupling scheme. This energy gap may then be determined accurately. As for the optical properties, they are characterized by the presence of a sharp and intense band at 422 nm; this formally spin-forbidden band for the Mn(II) chromophore is activated by an exchange mechanism. It corresponds to the transition between the $S = 2$ ground pair state and the $S^* = 2$ excited pair state in which the Mn(II) ion has an $^3/_2$ local spin. The intensity of this band only depends on the thermal population of the $S = 2$ state. Therefore, the temperature dependence of the intensity also leads to the energy gap between the low-lying states, irrespective of any spin-coupling scheme. The fact that the two techniques give the same value of the interaction parameter within the experimental uncertainties makes us confident in the optical technique and encourages us to investigate the optical properties of more complex $Mn^{II}Cu^{II}$ systems. Actually, all of the $Mn^{II}Cu^{II}$ systems we synthesized so far show a narrow and intense band between 400 and 425 nm, provided that the organic part of the molecule contains no aromatic ring. We will report soon on findings concerning tri- and tetranuclear species and one-dimensional ferrimagnets.

We would like to emphasize also that our MnCu compound displays a particularly well-resolved $S = 2$ EPR spectrum. A single-crystal EPR investigation is under way. Finally, owing to its relative simplicity, this MnCu compound may be also utilized to obtain new information on the mechanism of the Mn(II)–Cu(II) interaction through bisbidentate bridges. The distribution of the spin density on both the metal centers and the bridge would be particularly informative, and we hope to be able to carry out a polarized neutron diffraction investigation in the near future.

Acknowledgment. We are most grateful to D. Vivien, who put at our disposal his powder EPR simulation program, and to Y. Journaux for very useful discussions and advice concerning the EPR spectra.

Supplementary Material Available: Tables SI–SIV, listing detailed crystallographic data, anisotropic temperature factors, hydrogen coordinates and thermal parameters, and bond distances and angles within the triflate ion (4 pages). Ordering information is given on any current masthead page.

(51) Liao, D. Z.; Juan, S.; Jiang, Z. H.; Yan, S. P.; Cheng, P.; Wang, G. L. *Polyhedron* **1992**, *11*, 2621.